Supporting Information

Gonzalez-Perez et al. 10.1073/pnas.1322123111

SI Materials and Methods

Measurement of Run-Down and Analysis of Conductance–Voltage Curves. Ca^{2+}- and voltage-activated K^+ (BK) channels were expressed in *Xenopus* oocytes. To define the loss of γ1-mediated shifts after patch excision, patches were initially excised into a 10-μM Ca^{2+} solution, thus allowing determination of the conductance-voltage (GV) characteristics before any ostensible run-down. The patch was then exposed to one of three different run-down conditions that were tested (condition 1: 0 Ca^{2+}, 0 mV; condition 2: 10 μM Ca^{2+}, 0 mV; condition 3: 0 Ca^{2+}, +80 mV) for a 2-min interval before return to 10 μM Ca^{2+} to monitor the status of the GV curve. Elapsed times during run-down experiments reflect the cumulative time in the run-down condition. To define the shift, we monitored the time course of appearance of a component of channels with a V_h (the voltage at which BK channels are half activated) for activation indistinguishable from native Slo1 channels, which we term the unshifted component. Thus, irrespective of the behavior of the shifted portions of channels, the appearance of the unshifted component reflects the fraction of channels for which there is no residual γ1 effect. For analysis of the run-down time course, we only used patches that lasted long enough that the unshifted component reached a fractional value of at least 0.72. Such patches provided a minimum of four points for evaluation of the run-down time course, while also ensuring that we had sufficient patches for analysis.

In experiments in which α-subunits were titrated with various amounts of γ1-subunits, we evaluated a variety of fitting procedures. As shown in our examples in Figs. 1 and 2, a two-component Boltzmann function $\left[G(V) = G_s\left(\frac{1}{1+e^{\frac{z_1F(V-V_s)}{RT}}}\right) + G_u\left(\frac{1}{1+e^{\frac{z_2F(V-V_u)}{RT}}}\right)\right]$, where G_s represents the shifted fraction of conductance of V_s as the shifted voltage of half activation, and G_u and V_u reflect the unshifted fraction. z_1 and z_2 are the terms for voltage-dependence. Typically, z_1 and z_2 were constrained to be identical. We also tested whether additional Boltzmann components might improve the quality of the fits to such data but observed no improvement in fit quality by adding additional components.

Model Predictions. Predictions for binomially predicted fractional occupancies of channels with γ1-subunits under different models of assembly were generated using Mathcad 15 (PTC). Predictions for GV curves based on a given fractional occupancy were based on the summation of Horrigan-Aldrich predictions for the GV for each individual stoichiometric contribution, also generated with MathCad 15. Standard values for allosteric constants (1) were used for these calculations: $L = 10^{-6}$, $z_L = 0.3e$, J0 = 0.03, $z_J = 0.58e$; D = 25, C = 8, K = 11 μM, E = 2.4. For simulations of incremental and all-or-none gating shifts in which changes in a single allosteric constant were assumed to a given modulatory effect of an auxiliary subunit, a minimal (min) and maximal (max) parameter value were used. For D, $D_{min} = 25$ and $D_{max} = 425$, consistent with estimates of γ1 induced effect on D (2); for L, $L_{min} = 10^{-6}$ and $L_{max} = 400 \times 10^{-6}$; for J0, $J0_{min} = 0.03$ and $J0_{max} = 0.83$; for C, $C_{min} = 8$ and $C_{max} = 32$. For L, J0, and C, maximum values were simply chosen to produce maximal GV shifts of magnitude comparable to that observed with γ1-subunits.

Chemicals. Salts and buffers were obtained from Sigma. Mg^{2+}-ATP was from Sigma. Solutions of natural phosphatidylinositol 4,5-bisphosphate (PIP_2) from brain (Avanti Polar Lipids) or synthetic diC16- PIP_2 or diC8-PIP_2 (Echelon Biosciences) were prepared by initially dissolving in water at 1 mM and stored as aliquots. Before the experiments aliquots were dissolved in working solution to make 10 or 25 μM final concentrations.

1. Horrigan FT, Aldrich RW (2002) Coupling between voltage sensor activation, Ca^{2+} binding and channel opening in large conductance (BK) potassium channels. *J Gen Physiol* 120(3):267–305.

2. Yan J, Aldrich RW (2010) LRRC26 auxiliary protein allows BK channel activation at resting voltage without calcium. *Nature* 466(7305):513–516.

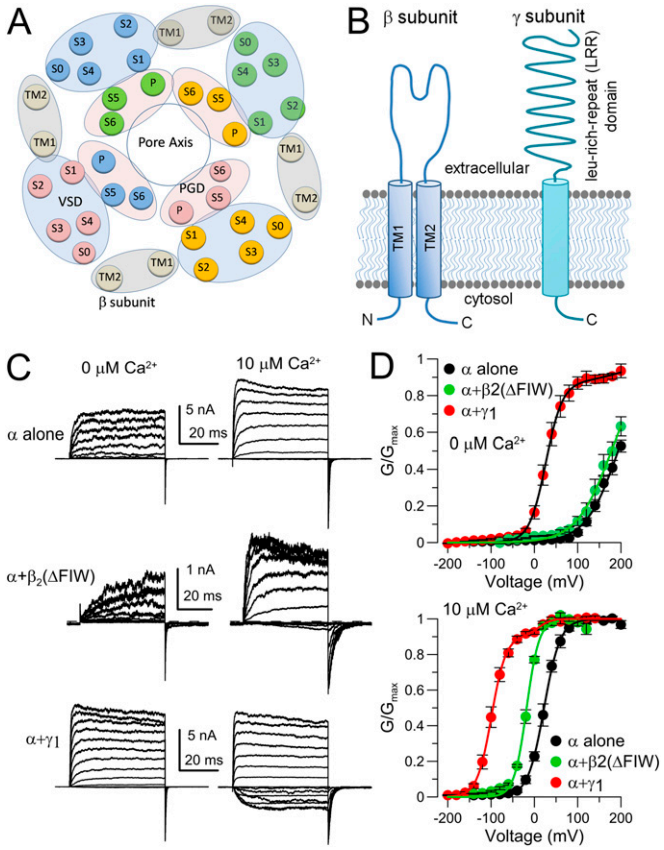

Fig. S1. Two distinct types of auxiliary subunits of BK channels, γ1 and β, produce robust shifts in gating. (*A*) Schematic of deduced positions (1, 2) of α- and β-subunit transmembrane (TM) segments at the extracellular face. TM segments for a given α-subunit share an identical color. Pink ellipses highlight pore-gate domain (PGD) elements; blue ellipses highlight voltage-sensor domain (VSD) elements; gray ellipses highlight β-subunits. (*B*) Cartoons of the topology of β2- and γ1-subunits highlighting N termini (NT), cytosolic C termini (CT), and extracellular domains. (*C*) Current activation over voltages from −200 to +200 mV at 0 and 10 μM Ca^{2+} for α-subunit alone (*Top*), α+β2(ΔFIW) (*Middle*), and α+γ1 (*Bottom*). (*D*) GV curves from sets of currents as in *C* at 0 Ca^{2+} (*Upper*) and 10 μM Ca^{2+} (*Lower*) for α alone (black), α+β2(ΔFIW) (green), and α+γ1(red), highlighting the more than 100-mV leftward shift in V_h produced by γ1 at both 0 and 10 μM Ca^{2+}, whereas β2 produces no shift at 0 mV relative to α alone, but an ∼50-mV shift at 10 μM Ca^{2+}.

1. Wu RS, Marx SO (2010) The BK potassium channel in the vascular smooth muscle and kidney: α- and β-subunits. *Kidney Int* 78(10):963–974.
2. Liu G, et al. (2010) Location of modulatory beta subunits in BK potassium channels. *J Gen Physiol* 135(5):449–459.

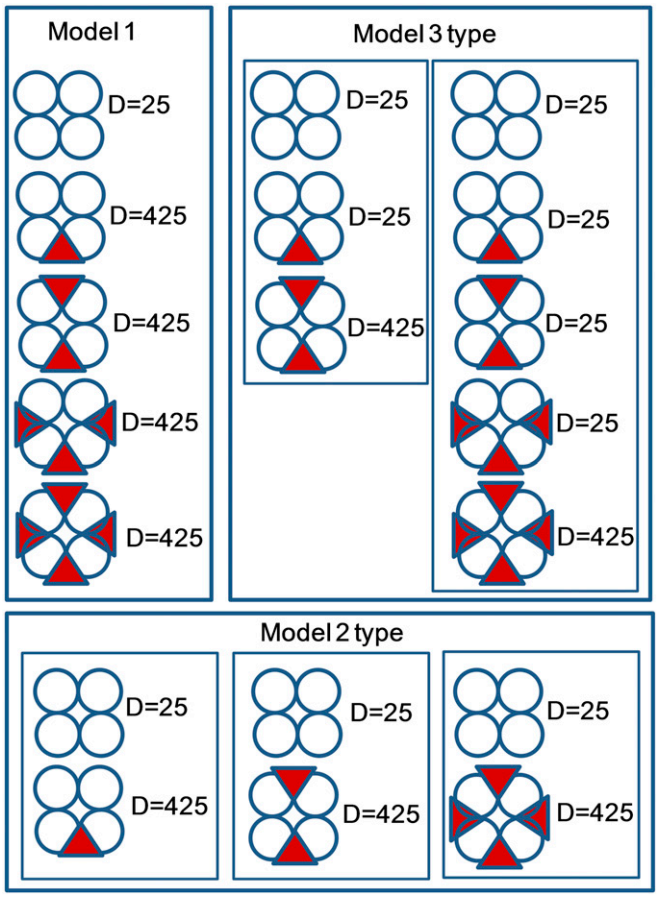

Fig. S2. Possible stoichiometric combinations of γ1:α-subunits that could underlie all-or-none gating shifts. Model 1 allows one to four auxiliary subunits per channel, but one subunit is sufficient to produce a full change in a given allosteric constant. Here the value for the allosteric constant D in relation to a given subunit combination reflects an all-or-none effect on that parameter when a single auxiliary subunit is present. Model 1 would also include a version in which only up to two γ1-subunits can assemble in a channel, but one is sufficient to produce a full effect on an allosteric constant. Model 2 allows a single γ1-subunit (or γ1-subunit complex) to assemble per channel, such that an all-or-none change in an allosteric constant occurs for channels associated with the full γ1 complex. Model 3 represents a case when up to some number of γ1-subunits can be present in a channel complex, but the gating shift only occurs when all required subunits are present.

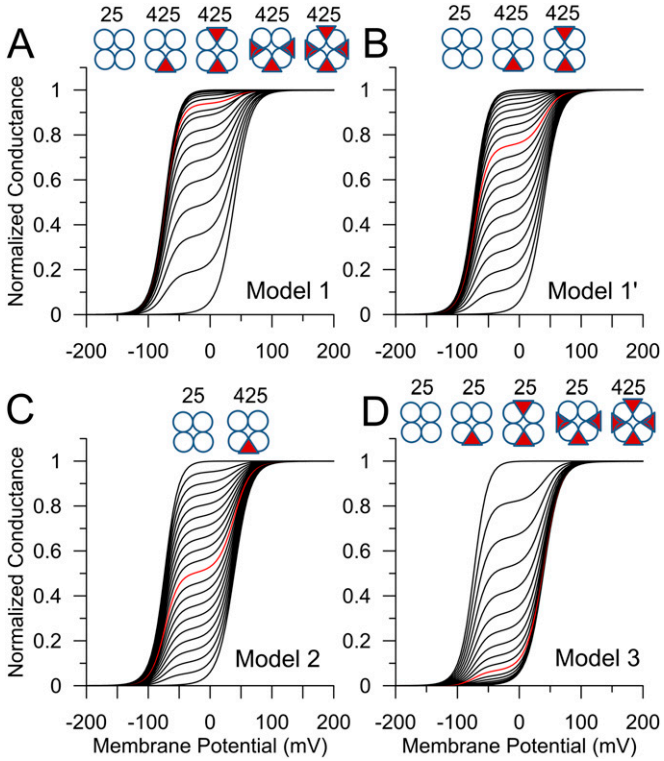

Fig. S3. Model-dependent changes in GV curves based on specific γ1:α-subunit stoichiometries. (*A*) GV curves were generated for different γ1:α fractional occupancies for model 1, with the indicated D value associated with a given stoichiometric combination. Red line corresponds to an average occupancy of two γ1-subunits per BK channel. (*B*) GV curves were generated for model 1 but with a maximum of up to two γ1-subunits per channel. (*C*) Calculated GV curves were based on model 2, in which only a single γ1-subunit associates per channel. (*D*) GV curves were based on model 3, in which one to four subunits can coassemble, but the gating shift only arises when all four γ1-subunits are present.

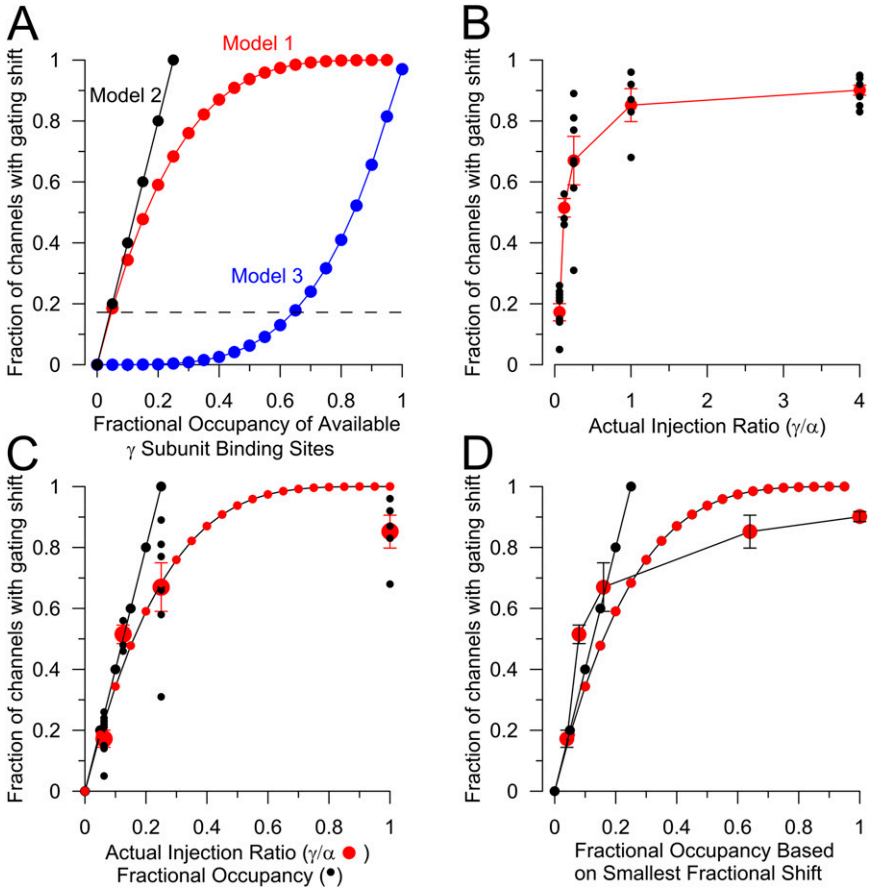

Fig. S4. Predictions for variation of fraction of shifted channels in accordance with γ1-subunit occupancy of channels. (*A*) Predictions of the fraction of channels exhibiting a full γ1 gating shift in accordance with channel occupancy by γ1-subunits are plotted for three distinct models. Model 1 (red): a BK channel can contain one, two, three, or four γ1-subunits, but one subunit is sufficient to produce a full gating shift. Model 2 (black): a BK channel can contain only one subunit per channel, and one is sufficient to produce the full gating shift. Because in this model only one γ1-subunit assembles with four α-subunits, the fractional occupancy only reaches 0.25 of the total potential sites per channel. Model 3 (blue): up to four γ1-subunits can coassemble, but a gating shift only occurs for channels with four γ1-subunits. The dotted line indicates the minimal level of fractional shift that was experimentally observed (0.17) over this set of injection ratios. The intersection of this line with the predictions for a given model provide an estimate of the actual mole-fraction of channel occupancy by an auxiliary subunit necessary to achieve that level of fractional shift. (*B*) Variation in the fraction of channels with a full gating shift as a function of the γ1:α injection ratio, with black dots as individual patches and red dots as means. (*C*) Comparison of observed fractional shifts to predictions of models 1 and 2, making the assumption of direct equivalence of injection ratio to fractional occupancy. (*D*) Relationship of observed fractional shift (large red symbols) to model 1 (red) and model 2 (black) based on renormalization of injection ratios to actual fractional occupancy. Renormalization is based on the idea that the fractional shift observed at the 1:16 γ1:α injection ratio defines the fractional occupancy for a given model. Because of the similarity in initial slope of the predicted shift vs. fractional occupancy for both model 1 and model 2, the 1:16 γ1:α predicts a similar fractional occupancy, 0.04 and 0.0425, respectively. For model 3, to obtain an observed fraction of shifted channels of ~0.17, γ1-subunits would occupy approximately 0.65 of the potential sites. A further doubling in fractional occupancy at the twofold higher injection ratio would therefore predict a maximal gating shift. On the basis of this, model 3 seems unlikely to be suitable.

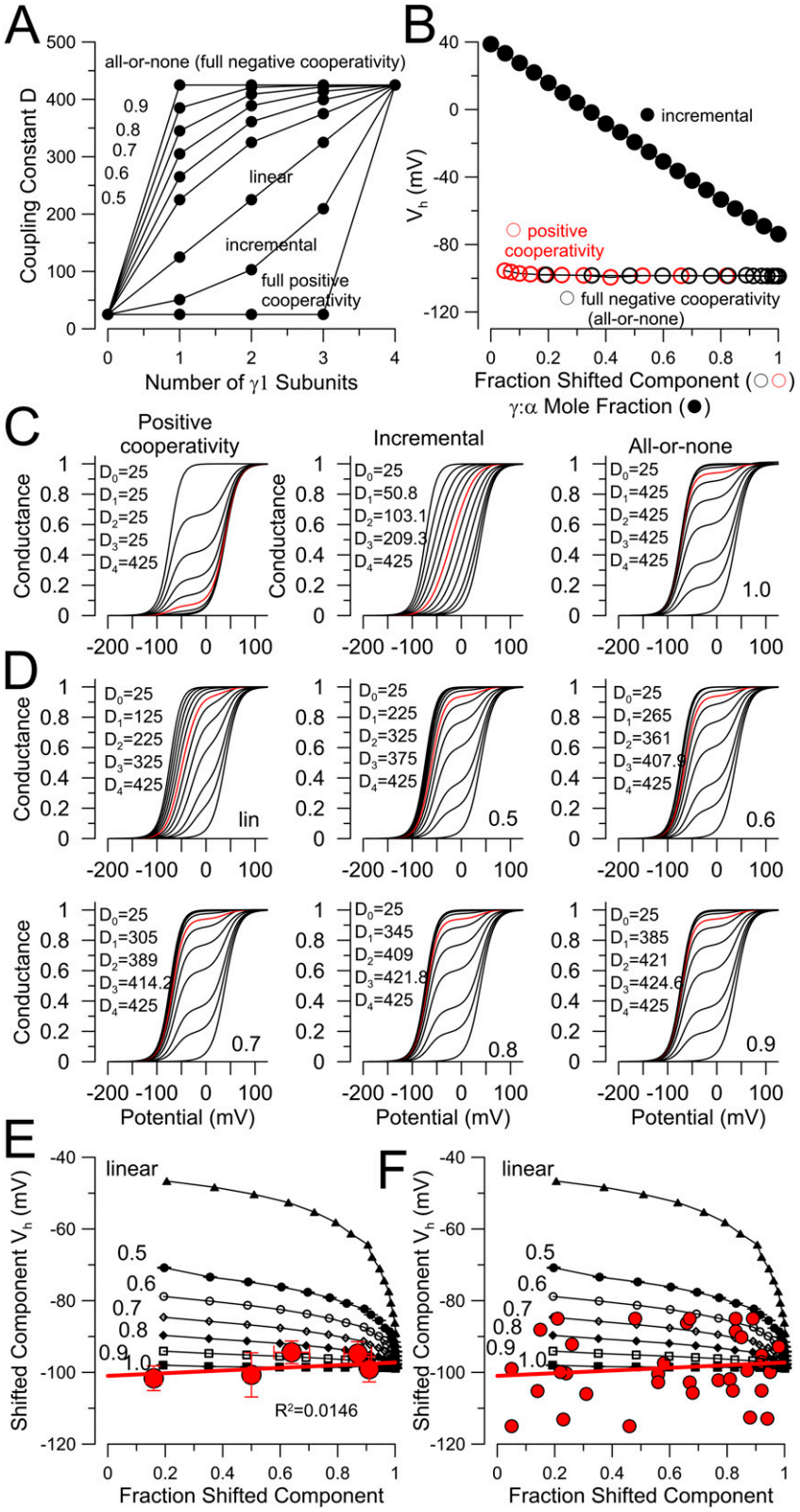

Fig. S5. For a model involving none to four γ1-subunits, the observed functionally all-or-none nature of γ1-mediated shifts would be indistinguishable from strong negative cooperativity. (*A*) Values of the average per-subunit coupling constant D for various assumptions of how D changes as a function of number of γ1-subunits per channel. For a full all-or-none effect, a single γ1-subunit results in D = 425. The incremental case is as in earlier figures. Full positive cooperativity corresponds to model 3 (Fig. S2). Cases indicated by linear and 0.5–0.9 correspond to different ad hoc assumptions about how additions of up to four γ1-subunits impact on D. We know of no theoretical framework for predicting exactly how a single γ1-subunit interacting with a single α-subunit might be expected to influence the energetics of adjacent subunits. For the cases shown, the fractional values correspond to the fractional impact a single γ1-subunit has of the full gating shift resulting from four γ1-subunits. (*B*) For all-or-none and positive cooperativity cases, the expected behavior of the shifted V_h is plotted as

Legend continued on following page

a function of fraction of that shifted component (based on simulations in *C*). For the incremental case, only a single V_h is measured (*C*, *Middle*), the V_h is plotted as a function of the mole-fraction of γ1:α for the simulation. Red curves correspond to 0.5 fractional occupancy by γ1-subunits. (*C*) Changes in GVs at different γ1-subunit mole-fractions are plotted for Positive cooperativity (model 3), Incremental, or All-or-none cases. (*D*) Changes in GVs at different γ1-subunit mole-fractions are plotted for other assumptions regarding the extent of negative cooperativity. (*E*) The V_h of the shifted component is plotted as a function of the fraction of that shifted component from the GV curves for the different assumptions of less than full negative cooperativity in *D*. Red symbols correspond to mean values of V_h of the shifted component and the fraction shifted component from Fig. 1 *C* and *D*, with respective SEM. (*F*) As in *E*, except individual estimates from all GV curves used in generation of Fig. 2 *C* and *D* are plotted. The data points were fit to a regression line yielding $R^2 = 0.0146$, suggesting that the shifted V_h does not shift appreciably with changes in fraction of the shifted component. This suggests that, for the case in which more than one γ1-subunits may coassemble in BK channels, the effect of a single γ1-subunit is indistinguishable from all-or-none and full negative cooperativity.

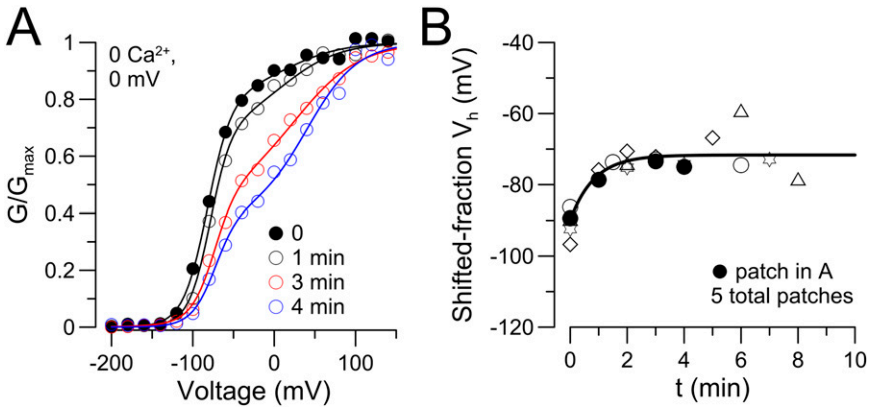

Fig. S6. Partial shifts may be associated with intermediate changes in γ1 effects. (*A*) During run-down, patches often show a small initial rightward shift in GV before obvious splitting into two components. (*B*) Fitted values of the shifted component at early times after excision reveal that the small rightward shift effect is complete within less than 2 min. Points are from five patches. Line is the fit of a single exponential with $\tau = 0.84 \pm 0.5$ min. Fitted V_h at t = 0 min is (−90.1 mV) and after the small shift, $V_h = -71.7 \pm 1.9$ mV.

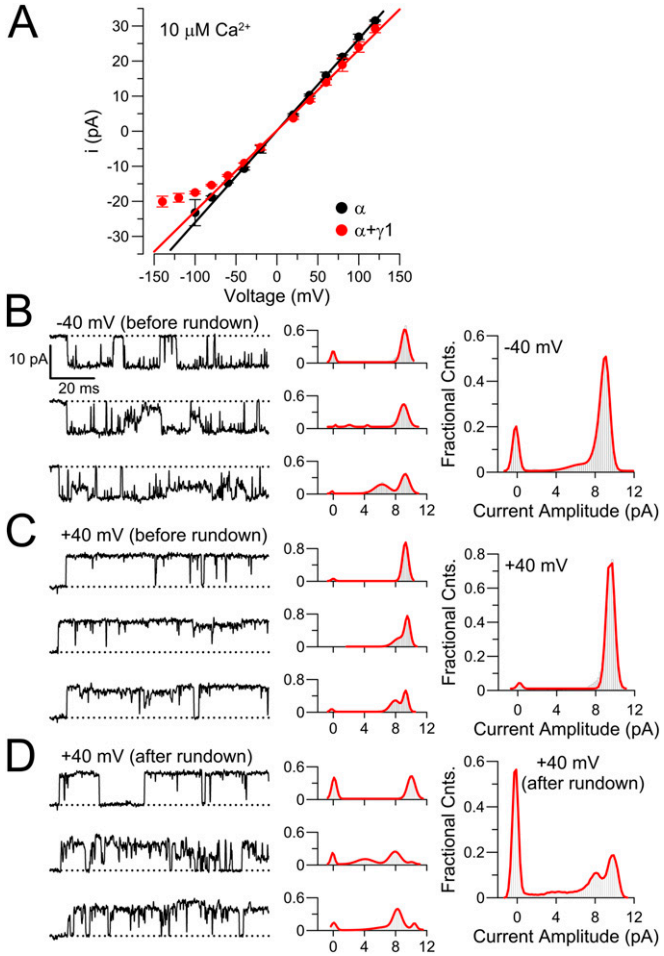

Fig. S7. Channels with γ1-subunits have a slightly reduced single-channel conductance and open to subconductance levels. (*A*) Mean single-channel current-voltage relationships for channels containing α-subunits alone and α+γ1-subunits with lines showing the fitted single channel conductance estimates of 261 ± 2.7 pS ($n = 3$ patches) and 230 ± 4.6 pS ($n = 4$ patches), respectively. For α+γ1, only the largest current level was used. (*B*, *C*, and *D*) Examples of openings and total amplitude histograms from a single α+γ1 channel recorded at negative (*B*, −40 mV) and positive (*C*, +40 mV) potentials, and then following the run-down associated change in Po vs. V (*D*, +40 mV). At each potential, a total of 20 sweeps were recorded. Among different voltages (−80, −60, −40, 40, 60, and 80 mV), typically 13–17 sweeps out of 20 show openings to a well-defined single main level of maximum conductance (upper traces in *B*, *C*, and *D*), whereas only 3–7 sweeps out of 20 show intermediate current levels (middle and bottom traces). Total amplitude histograms from each individual sweep (*Center*) or from a total 20 sweeps (*Right*) with fits to the sum of four gaussians (red line) confirm the presence of multiple levels of subconductance. Before run-down (*C*), subconductance excursions at more positive potentials open to a larger fraction of the main conductance than at negative potentials (*B*). However, the overall fraction of time in subconductances relative to the main conductance appears similar at positive and negative potentials based on open amplitude histograms for sets of 20 sweeps over a set of three patches. Subconductance behavior was also noted in channels after run-down (*D*). Three patches with α-alone channels did not exhibit such subconductance behavior, consistent with many earlier studies on BK channels.

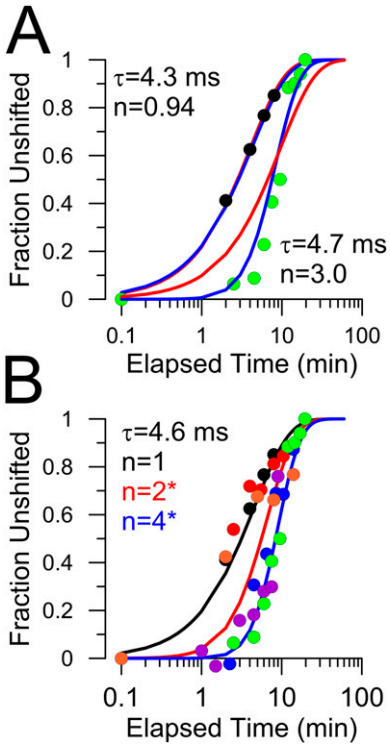

Fig. S8. The time-course of the loss of the γ1-induced gating shifts exhibits a lag, consistent with a stoichiometry of up to four steps required for run-down to occur. (*A*) Examples of the loss of gating shift for two individual patches, with fits of $f(t) = [1 - \exp(-t/\tau)]^n$, where τ is the time constant of a single γ1 becoming inactive, and *n* is the number of γ1-subunits. Values for τ and *n* are shown. Red curve corresponds to a fit with *n* constrained to one for patch with green circles. Both patches exhibit a comparable time constant but differ in terms of the apparent cooperativity. (*B*) Points are shown for six patches (each in a different color) that were maintained long enough to achieve run-down to values over 0.72. This extent of recovery ensured that at least four separate measurements of shifted and unshifted fractions were obtained. Three cells exhibit substantial delay in run-down consistent with *n* of 3–4, whereas, for three other cells, $n \sim 1$. Curves correspond to $n = 1$, 2, or 4, all with an average time constant (4.6 ± 0.7 min) derived from the mean of the set of five cells [one patch (orange symbols) with $\tau = 12.1$ min was excluded from the mean calculation].